SUPPLEMENTARY TABLES AND FIGURES

|	Hit Rates (%)			False Alarms (%)
	Cued	**Uncued**	**p-value**	**Overall**
Monkey L	83.9	71.5	<0.0001	10.0
Monkey R	79.1	64.7	<0.0001	9.9
Combined	81.5	68.1	<0.0001	9.9

Table S1. *Monkeys demonstrated significantly better behavioral performance (i.e., higher hit rates) at the cued location relative to an uncued location, Related to Figure 2.* The p-values are based on t-tests.
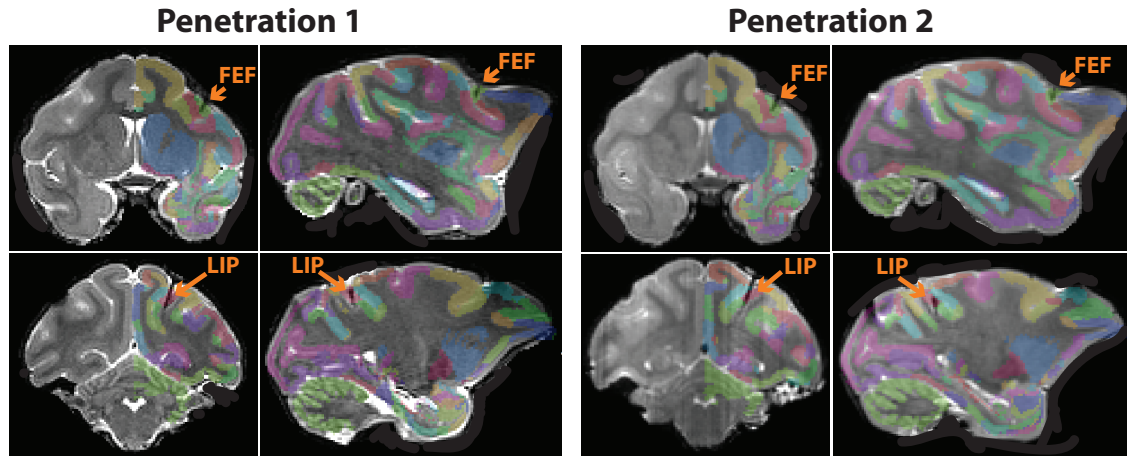
Figure S1. *For all recordings, electrodes were positioned in atlas-defined FEF and LIP, Related to STAR Methods.* Coronal and sagittal images from two electrode penetrations. Platinum-iridium electrodes create clearly visible "shadows," allowing for their localization in the ROIs. The colored regions overlaid on the T2-weighted structural images represent subdivisions of the anatomical atlas, including FEF (in green) and LIP (in red).
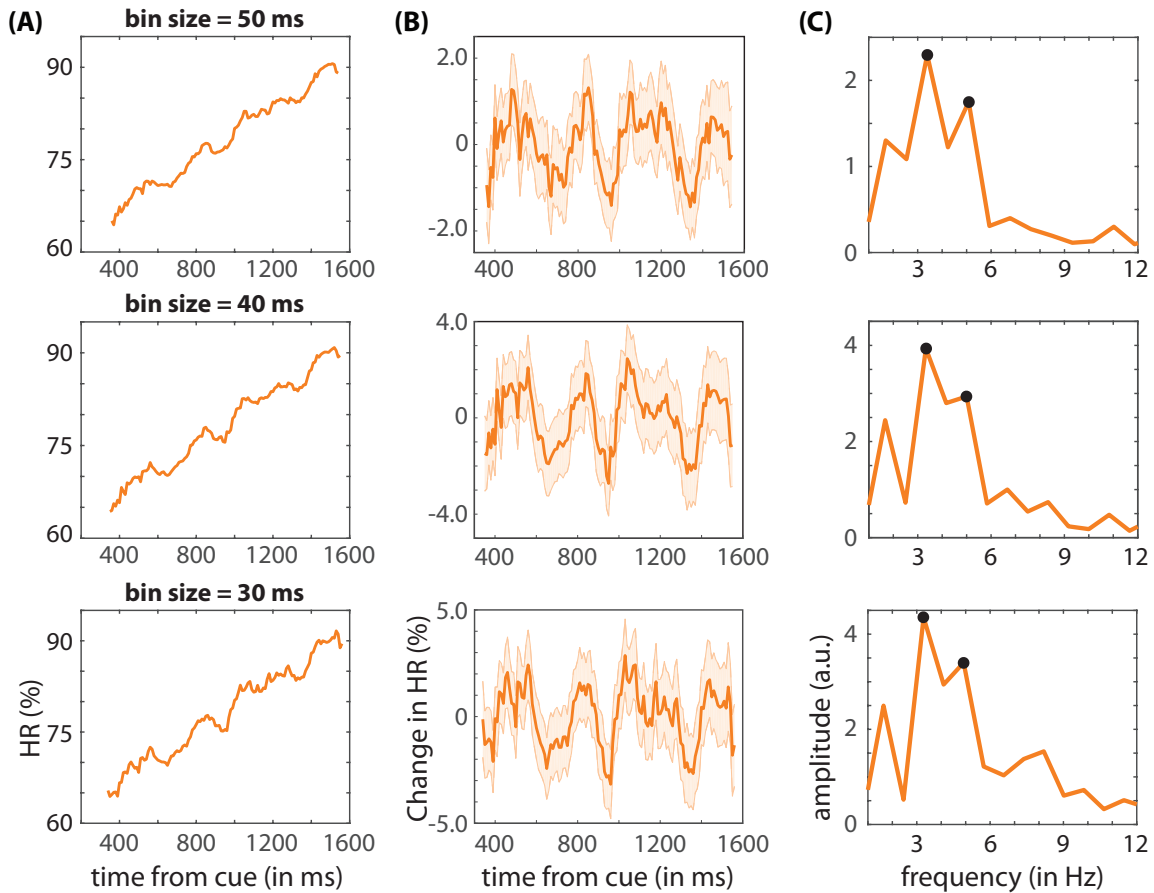
Figure S2. *Behavioral periodicity in the theta range (3–8 Hz) is independent of the length of the window (i.e., 30, 40, or 50 ms) used to bin trials, Related to Figure 2.* **(A)** Shows visual-target detection as a function of the time from cue, using different bin sizes to calculate HRs. Prior to calculating HRs, trials were binned using a sliding window (in 10-ms steps), with window lengths of 30, 40 or 50 ms. **(B)** These data were then linearly detrended, aiding visualization of the periodic effects. The shaded regions around the lines represent standard error of the mean. **(C)** The fast Fourier transform (FFT) was used to convert behavioral time-series data into the frequency domain. The black dots represent statistically significant peaks after corrections for multiple comparisons, demonstrating significant theta-band rhythmicity in monkey behavioral performance. Changing the length of the binning window did not change the pattern of the results or their statistical significance.
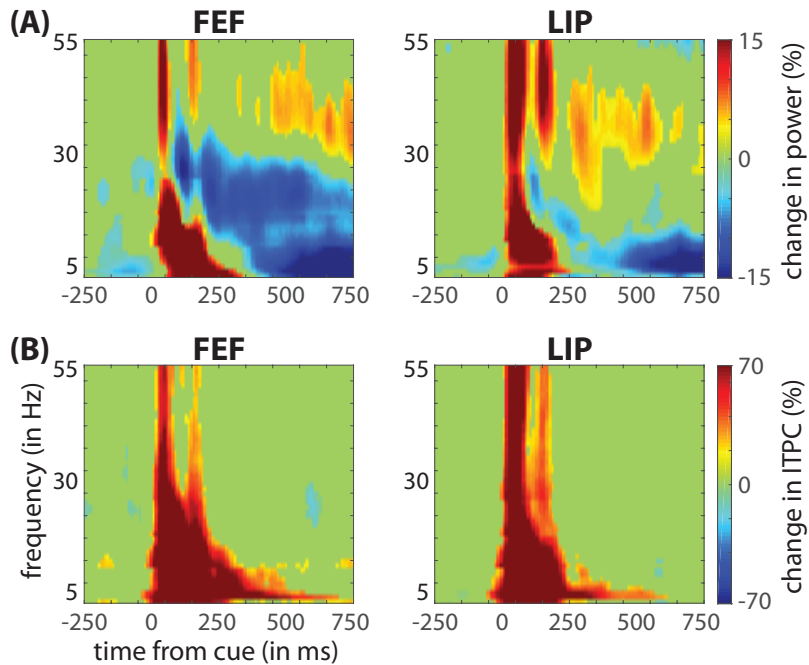
Figure S3. *Evidence of inter-trial phase consistency (ITPC) following the spatial cue, Related to Figure 2.* **(A)** Displays the cue-locked, percent change in power from baseline (-650 to -250 ms) when response fields overlapped the cued location. **(B)** Displays the corresponding cue-locked, percent change in ITPC from baseline. Insignificant changes from baseline, either positive or negative, have been zeroed. That is, all values greater than or less than zero are statistically significant (p < 0.0005; permutation statistics). There is a significant increase in ITPC (from baseline) at low theta frequencies (in both FEF and LIP) that outlasts the initial cue-evoked change in theta power.
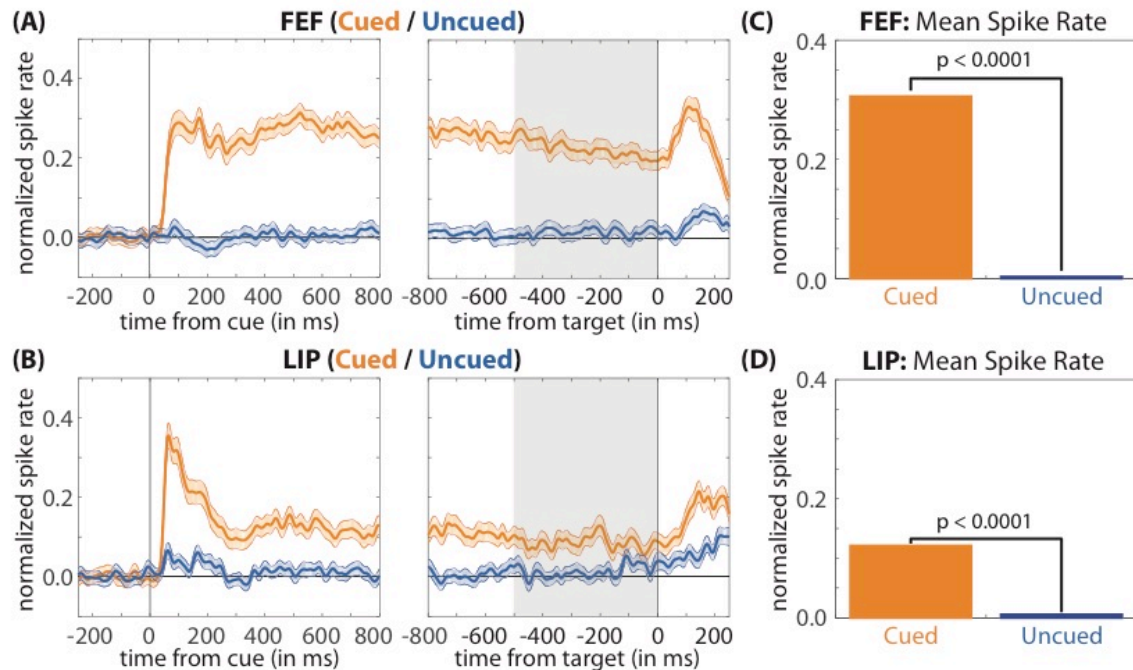
Figure S4. *Neurons in both FEF and LIP demonstrate significantly increased spiking activity during the cue-target delay (i.e., under conditions of covert, sustained spatial attention), Related to Figure 2.* Population PSTHs averaged across all neurons in **(A)** FEF (N = 81) and **(B)** LIP (N = 80) with significant responses to the cue (or both the cue and the target). Normalized spike rates under conditions of covert, sustained spatial attention (orange line) are compared with normalized spike rates outside the focus of spatial attention (blue line). Shaded regions around the lines represent standard error of the mean. For statistical testing, data were averaged over a 500-ms window that preceded target presentation (shaded in gray). **(C, D)** Provide the results of that averaging for each cortical region by attention condition (cued vs. uncued) and the p-values for the between-condition comparisons (Wilcoxon rank-sum test).
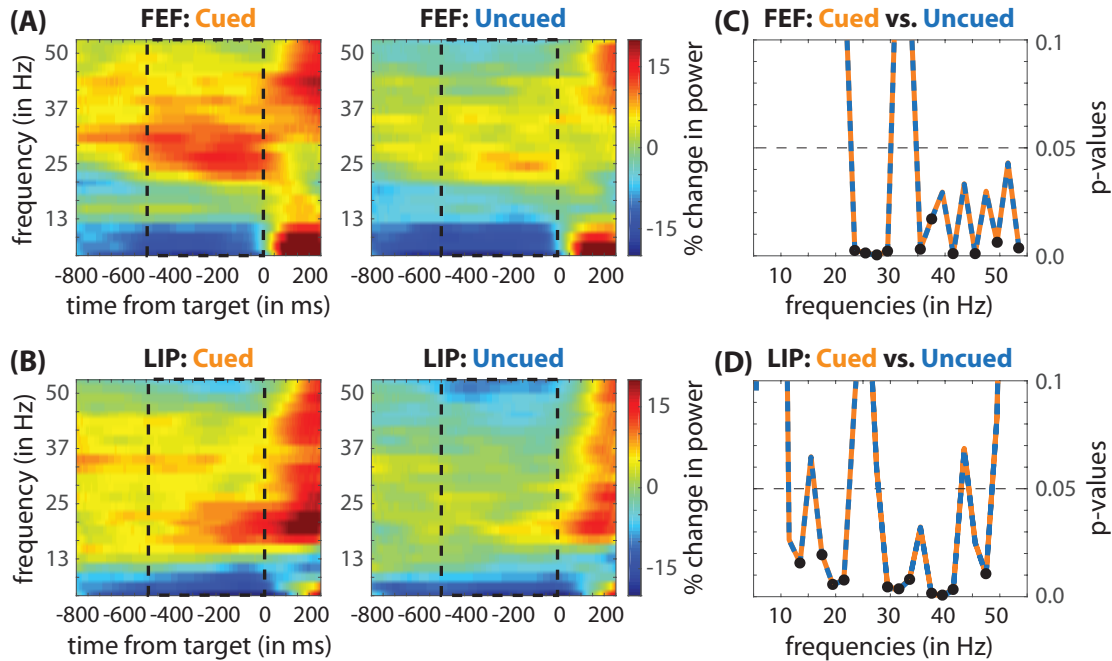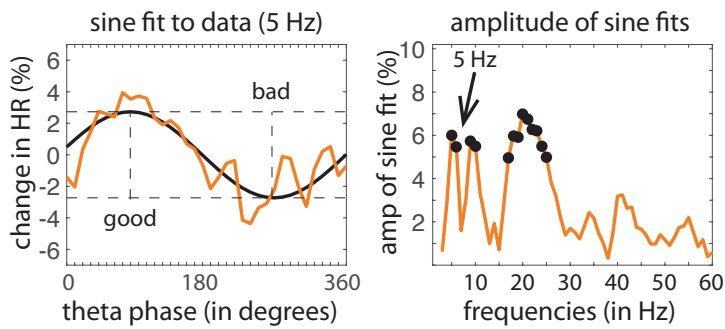
Figure S5. *Changes in the LFP signal following the spatial cue demonstrate attention-related effects in both FEF and LIP, Related to Figure 2.* **(A, B)** Target-locked spectrograms illustrate changes in oscillatory power under conditions of sustained, covert spatial attention (i.e., when response fields overlapped the cued location) relative to changes in oscillatory power outside the focus of spatial attention (i.e., when response fields overlapped the uncued location). These changes in oscillatory power are visualized as a percent change relative to a pre-cue baseline period (from -250 to -50 ms before cue presentation). For statistical testing, data were averaged over a 500-ms window that preceded target presentation (outlined with a dashed line). **(C, D)** The statistical significance of between-condition comparisons is illustrated with p-values (Wilcoxon rank-sum test). The black dots represent significant findings after corrections for multiple comparisons.
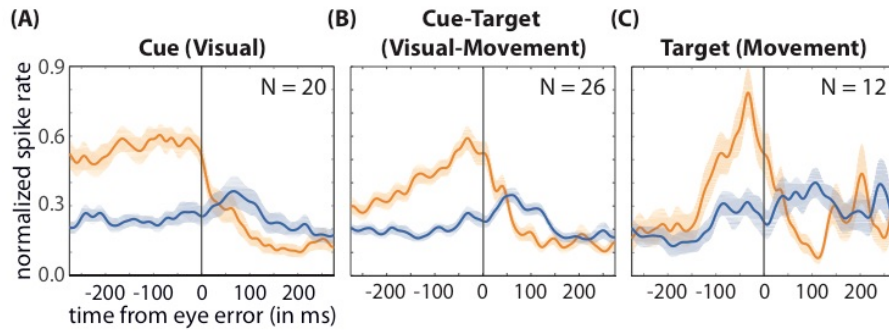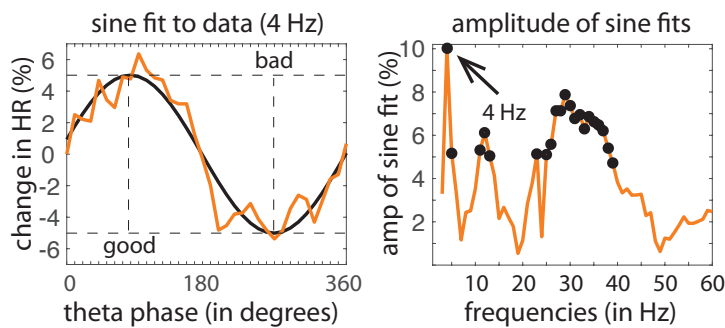
Figure S6. *Neurons with target responses also demonstrated saccade-related activity, Related to Figure 6.* Population PSTHs time-locked to eye-movement errors during the cue-target delay for **(A)** cue-responsive, **(B)** cue-target-responsive, and **(C)** target-responsive neurons. Comparisons between when the cue occurred either within the receptive field (orange line) or outside the receptive field (blue line). Shaded regions around lines represent standard errors of the mean.

**(A) FEF: Phase-Detection Relationships (3–60 Hz)**

sine fit to data (5 Hz)

amplitude of sine fits

(B) LIP: Phase-Detection Relationships (3–60 Hz)

sine fit to data (4 Hz)

amplitude of sine fits

Figure S7. *Oscillatory phase in both FEF and LIP modulates behavioral performance, regardless of the size of the phase bins used to measure phase-detection relationships, Related to Figure 3.* Figure 1 presented phase-detection relationships that were estimated using 180° phase bins (i.e., hit rates were calculated within phase bins spanning 180°). **(A, B)** Provide parallel results that were instead estimated using 90° phase bins. These results demonstrate that the present findings were not dependent on bin size. The black dots represent statistically significant findings after corrections for multiple comparisons.
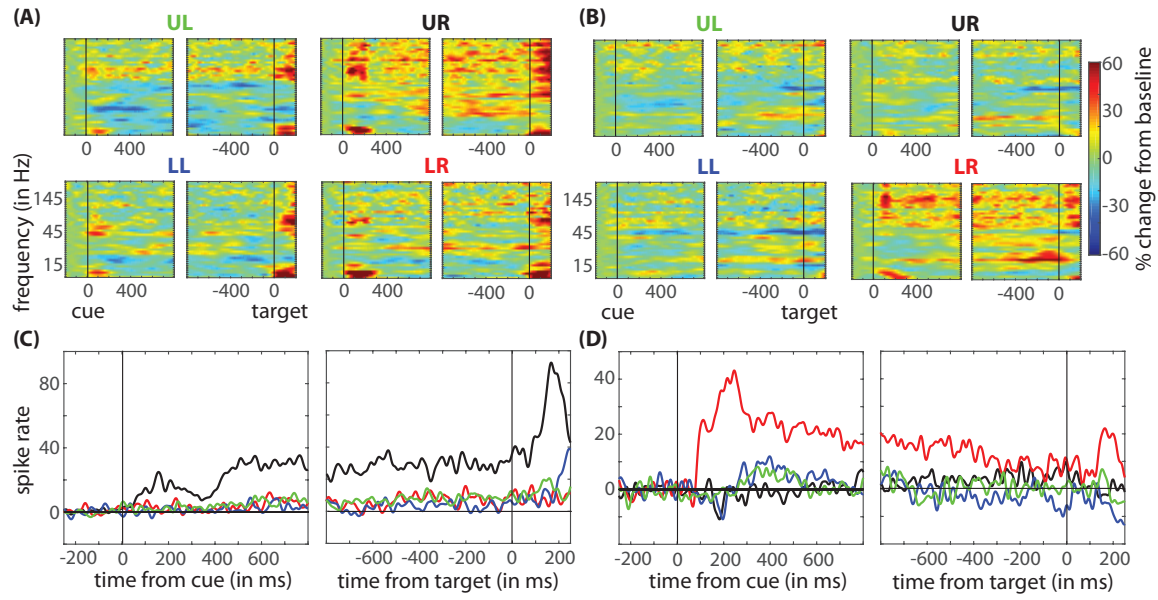
Figure S8. *Receptive fields and response fields were typically strongly biased toward stimuli within a single visual quadrant, Related to STAR Methods.* **(A, B)** Spectrograms (i.e., LFPs) and **(C, D)** spike rates from two recording sessions in FEF. **(A, B)** Spectrograms are presented by visual quadrant, in which the cued occurred. Left panels: Time 0 is aligned to cue onset; right panels: time 0 is aligned to target onset. **(C, D)** For spike rates: upper right (UR) = black, lower right (LR) = red, lower left (LL) = blue, and upper left (UL) = green.
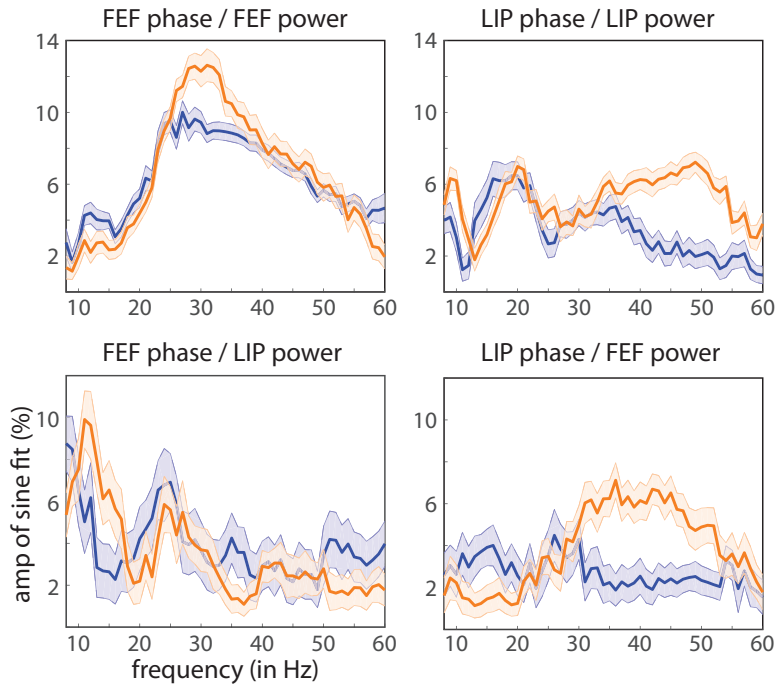
Figure S9. *Between-condition differences in phase-amplitude coupling (PAC) are still present after equating both theta power and higher-frequency power across the two conditions (cued vs. uncued), Related to Figure 4.* We used a stratification procedure that involves subsampling the original dataset to equate power, meaning that the results vary somewhat on each run. We therefore ran 1500 iterations of the stratification procedure (separately for PAC in FEF, LIP, FEF/LIP, and LIP/FEF). The above plots (comparable to the plots in Fig. 4B, D) provide the mean and standard deviation of those power-equating iterations, comparing the strength of PAC when response fields overlapped either the cued location (in orange) or the uncued location (in blue). These results confirm the between-region findings presented in Figure 4.
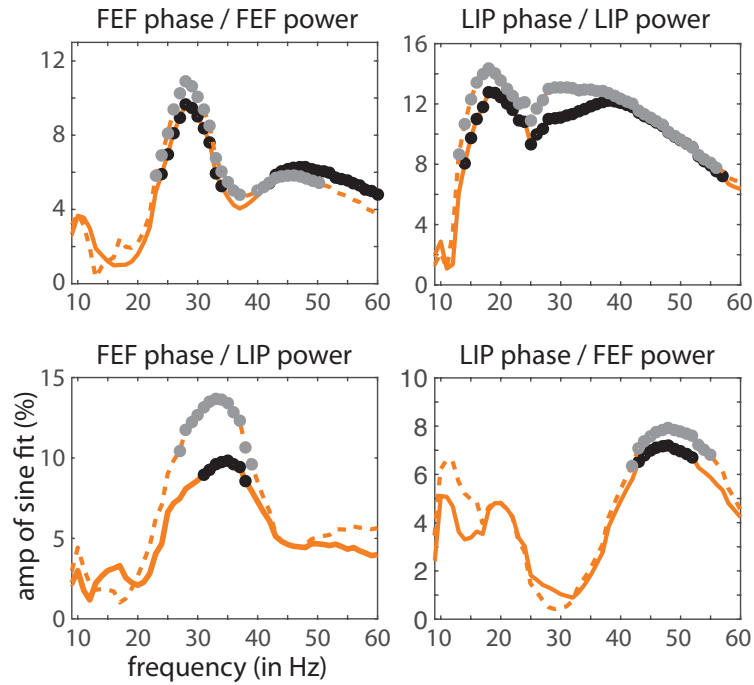
Figure S10. *The strength of phase-amplitude coupling (PAC) before and after eliminating trials with microsaccades during the cue-target delay, Related to Figure 4.* These results (comparable to the plots in Fig. 4B, D) are based on a subset of recording sessions where eye position was sampled at a high enough rate to detect microsaccades (N = 30 for FEF, N = 32 for LIP, N = 22 for FEF and LIP). The dashed lines represent the strength of PAC after eliminating trials with microsaccades. Despite using fewer trials, both within- and between-region PAC remained statistically significant, with significant findings indicated by either gray (without microsaccades) or black circles (with microsaccades).
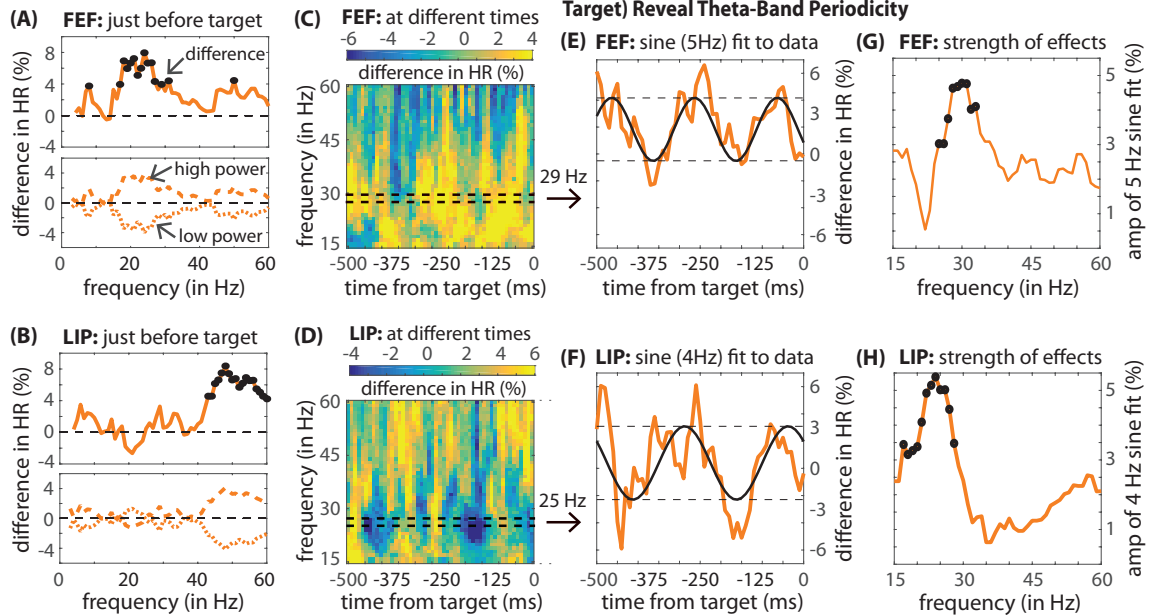
Figure S11. *Relationships between oscillatory power and hit rates (during spatial attention) are consistent with an ongoing, periodic process with theta-band rhythmicity, Related to Figure 4.*

(A, B) Oscillatory power (from 3–60 Hz), just prior to target presentation, was split into low- and high-power bins (based on median power), and then HRs were calculated for each of those bins. **(C, D)** These power-detection relationships (from 15–60 Hz) were then estimated at different times relative to target presentation. That is, we examined whether power at different time points (from -500 ms to 0 ms) prior to target presentation was predictive of visual-target detection. **(E, F)** Power-detection relationships fluctuated as a function of time from target, demonstrating theta-band rhythmicity. The amplitude of multi-cycle sine waves (in black) provided the strength of this theta-band rhythmicity **(G, H)** for temporal fluctuations in power-detection relationships from 15–60 Hz. The black dots represent statistically significant findings after corrections for multiple comparisons. We hypothesize that these temporal fluctuations in power-detection relationships reflect the alternating, theta-organized attentional states described throughout the paper. That is, power at -450 ms (high vs. low) is not directly related to subsequent behavioral performance, but rather it is indicative of the attentional state that ultimately occurred at target presentation (rhythmically alternating between "good" and "poor", with "good" ultimately coinciding with target presentation).
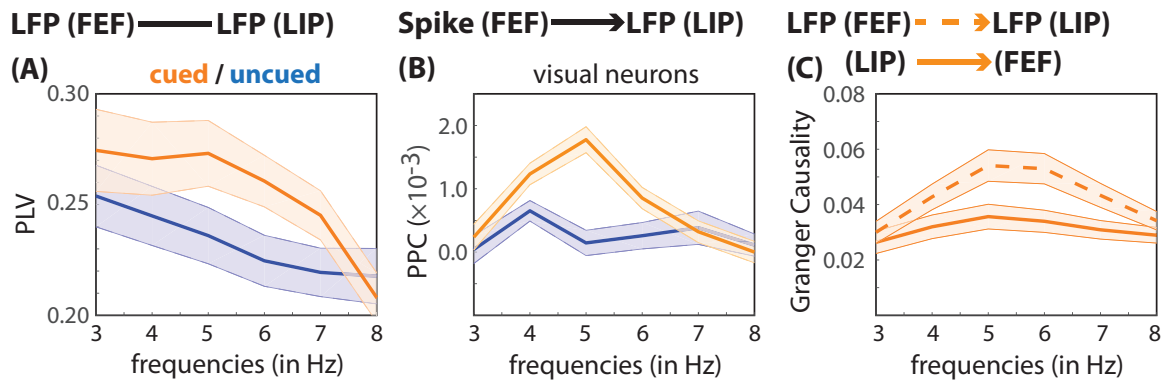
Figure S12. *Between-condition differences in three measures of FEF-LIP synchronization are still present after equating power across conditions, Related to Figure 5.* We used a stratification procedure that involves subsampling the original dataset to equate power, meaning that the results vary somewhat on each run. We therefore ran 1000 iterations of the stratification procedure. The above plots provide the mean and standard deviation of those power-equating iterations. **(A)** Compares LFP-LFP phase coupling when response fields overlapped either the cued (in orange) or the uncued location (in blue), **(B)** compares spike-LFP phase coupling when receptive/response fields overlapped either the cued or the uncued location, and **(C)** compares the relative influence of each cortical region on theta-band activity in the other cortical region (i.e., by measuring Granger causality). These results confirm the between-region findings presented in Figure 5.
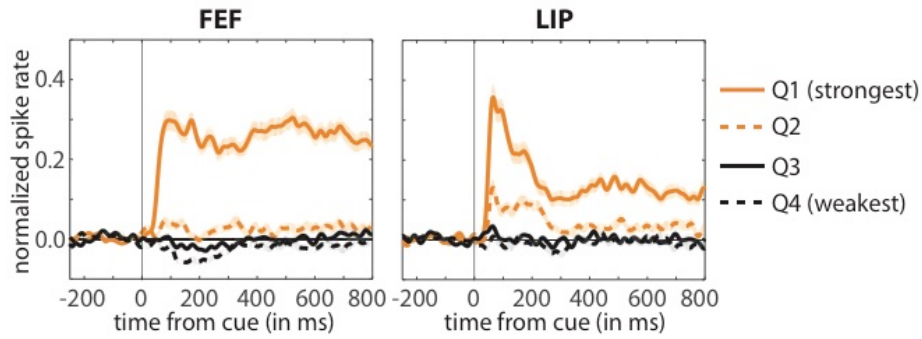
Figure S13. *Across all neurons, receptive fields were strongly biased toward stimuli within a single visual quadrant for both FEF and LIP, Related to STAR Methods.* Population PSTHs for neurons with a significant response to the cue. Prior to averaging, neurons were sorted based on their responses to cues in each visual quadrant. The solid orange line, for example, represents normalized spike rates following cues that occurred in the visual quadrant (Q1) associated with the strongest neural response. The dashed orange line represents normalized spike rates following cues that occurred in the visual quadrant (Q2) associated with the second strongest neural response. Shaded regions around lines represent standard errors of the mean.
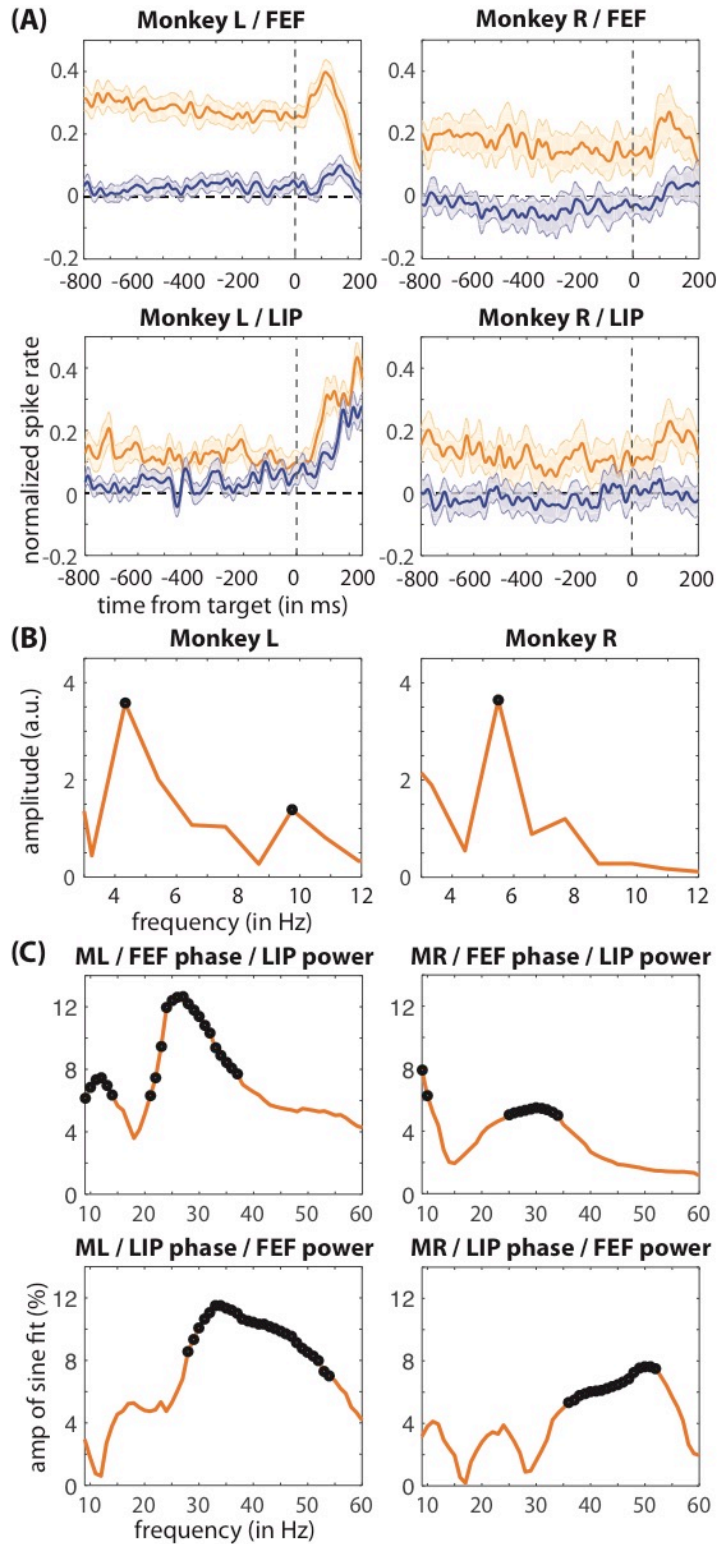
Figure S14. *Both monkeys demonstrated significantly better visual-target detection at the cued location (Table S1), (A) significantly increased spiking activity during the cue-target delay, (B) significant theta-band rhythmicity in their behavioral data, and (C) statistically significant phase-amplitude coupling, Related to STAR Methods.*